Journal of Wasit for Science and Medicine 2025: 18, (4), 32-44

Phenethylamine's Effect on Preventing the Corrosion of Low-Carbon Steel in Acidic Environments: Theoretical and Experimental DFT Computational Investigation

Samah Abbas Jihad, Israa Sattar Gatea, Aya Qasim Khanjar, Athra G. Sager, and Raheem A. H. Al-Uqaily

Chemistry Department, College of Science, Wasit University, Iraq.

Abstract

The current study employed polarization and gravimetric methods to investigate the corrosion resistance of low carbon steel in a solution with hydrochloric acid and different concentrations of phenethylamine. The inhibitor showed a high level of inhibitory effectiveness IE (%). Inhibitor's efficacy tends to decline with increasing temperature and concentration. The structure of inhibitor contains amine and ethyl groups, which are necessary for the adsorption process. These groups form a thin layer on the metal's surface and provide sufficient corrosion prevention. The thermodynamic parameters enthalpy, adsorption free energy, and entropy change were determined. Results were in line with previous research and were suitable. Adsorption and dissolution thermodynamic functions were also calculated. Moreover, DFT was used to compute thermodynamic functions of adsorption and dissolution for inhibitor. Also, energy levels of the least occupied molecular orbital (LUMO) and the energy of the most occupied molecular orbital (HOMO) were studied.

Keywords: Inhibition, Low carbon steel, DFT calculations.

1. Introduction

Rusting process is a significant issue in many industries. With an emphasis on how metals behave in various settings and corrosion-prevention strategies, scientists and engineers are investing heavily in corrosion research [1-3].

Mild steel is the most widely used metal alloy in the industrial industry for both construction and scientific research because of its low cost, high thermal and electrical conductivity values, strong mechanical qualities, and chemically stable weight percentages [3-5]. Sulfuric acid's cheaper cost and improved efficiency make it useful

for a variety of processes, including acid cleaning, petroleum etching, acid descaling and industrial cleaning.

Another possible solution to the industry's main corrosion prevention issue is the use of inhibitors to stop metals from oxidizing in acidic conditions [6-10]. Hydrochloric acid solutions were used in metal pickling and other industrial procedures readily erode metals. Inhibitors are among the most economical methods of slowing down the corrosion process on metal surfaces, especially in acidic settings [11-15].

In addition to preventing anodic or cathodic sites, inhibitors can shield metal surfaces against corrosive substances [16-20]. Adsorption processes of inhibitors govern effectiveness of corrosion inhibition, and these processes are mainly regulated by the interaction of the inhibitor's *F*-orbitals with the d-orbitals of the surface molecules, or the steric factors. Important factors to consider include the donor atoms' electrical density, aromaticity, and functional group. Corrosion inhibitors are found in both organic and inorganic materials [21-25].

Because of the heteroatoms in their lengthy chain structure, these compounds offer anti-corrosive properties. Among the main disadvantages of these inhibitors are their high cost and their toxicity, which makes them dangerous for both human beings and the environment. Steel is reduced to its mineral, such as oxide or hydroxide, or chemically stabilized throughout the corrosion process [20-25].

Conversely, metals corrode with time due to chemical reactions with its environment. Corrosion is the term used to describe the deterioration of metal structures caused by environmental exposure including pipelines, structures, metal bars, and frames [20-25]. A potent computational technique in quantum mechanics, density functional theory (DFT), were utilised to study the electron density rather than the intricate many-body wave function to ascertain the electrical structure and characteristics of molecules, atoms, and materials.

DFT calculation is a popular method in the fields of physics, chemistry, and material science, allows the investigation of bigger and more complicated systems with an optimal balance of computing cost and accuracy by reducing the issue to the significantly simpler 3D electron density [26-29].

2. Materials and Methods

2.1 Experimental work

Low carbon steel, which is composed of 0.13% C, 0.45 % Si, and 0.07 % P, was used in this experiment. Also, 0.06 % Al, 0.08 % Mn, and 0.05 % for S, and 0.05% for Fe.

Emery sheets were used to manually scrape the steel plates. The surface was cleaned and degreased using distilled water. This solution was made by diluting analytical-grade hydrochloric acid with distilled water.

This study employed weight loss and polarization techniques with varying inhibitor dosages of 100, 200, 300, and 400 ppm of phenethylamine in an electrochemical cell with three electrodes: reference electrode R.E., specimen electrode W.E and calomel electrode C.E [5-10].

2.2 Weight Loss Method

Weight loss measurements were conducted by immersing low-carbon steel coupon in acidic solutions for six hours at temperatures ranging from 30 to 50 ºC, where the weight loss was calculated and inhibition efficiency, furthermore the concentrations must normally be rather low (parts per million).

Both inhibitor-containing solution and uncontrolled (blank) solution were investigated. The following formula was used to determine the inhibitory efficiency (IE %) [11-18].

$$\% \text{ IE} = (W1\text{-}W2)/W1 \times 100$$

Where, W1 and W2 stand for the corrosion rates in the absence and presence of an inhibitor, respectively.

2.3 Electrochemical Method

Electrochemical measurements were performed using a conventional three-electrode cell consisting of a carbon steel working electrode containing WE, a platinum counter electrode, and a SCE reference electrode connected to a potentiated was used to conduct the electrochemical testing. 1 cm^2 of the WE surface is subjected to a 30-minute solution test to achieve a stable open circuit potential (ocp).

In order to change from the current's peak (Eocp) to either negative (cathodic reaction) or beneficial (anodic response), the voltage level was measured at a rate of 1 mV/s after the current peak (ocp). By using anodic and cathodic curves, the corrosion current density, or Icorr, were calculated using the following equation [17-22].

$$\eta\,\% = \frac{(\text{Icorr})\text{w} - (\text{Icorr})\text{i}}{(\text{Icorr})\text{w}} * 100$$

where (Icorr)w and (Icor)i represent the uninhibited and inhibited corrosion current densities, respectively [11-16].

3. Results and Discussion

3.1 Polarization Curves at Various Inhibitor Dosages, and Temperatures

The potential (mV) and current (A/cm^2) polarization curves at various inhibitor

dosages at 30 ºC are displayed in (figure 1). As a result, the anodic and cathodic curves may be displayed, showing a trend for corrosion potential and current densities to decrease as inhibitor concentrations increase.

Ecorr's cathodic and anodic combination, which yields the intended outcomes. Figures 2, and 3 show polarization curves, while (table 1) shows the improved efficiency findings at 40 and 50 ºC. The efficiency, corrosive potential, and current corrosion density all declined with increasing concentrations and temperatures. The study results were perfectly consistent with those of previous studies [12-19].

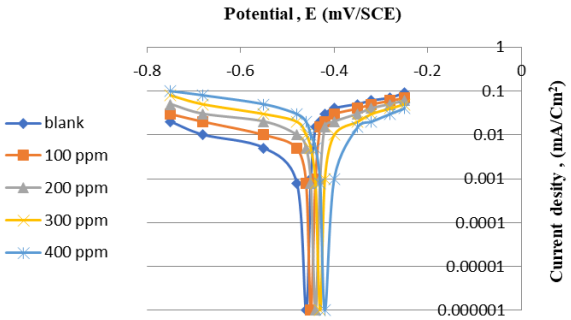

Figure1: Potential and current density polarization curves at 30 °C.

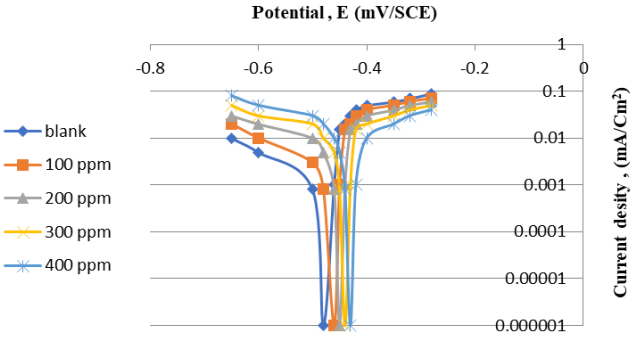

Figure 2: Potential and current density polarization curves at 40 °C.

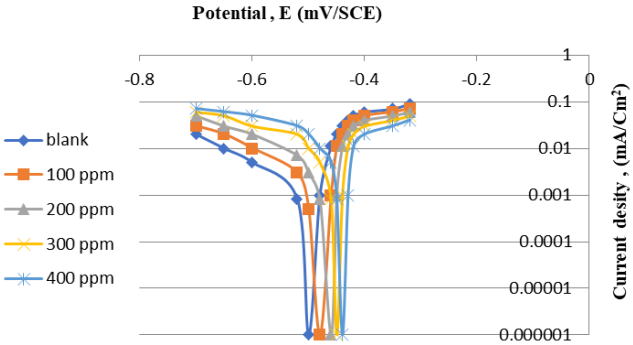

Figure 3: Potential and current density polarization curves at 50 °C.

Table 1: Icorr, Ecorr, inhibition efficiency for polarization method.

Inhibitor Conc. ppm	E corr (mV)			Corrosion current density (µA/cm²)			Efficiency of inhibition %		
	30 ºC	40 ºC	50 ºC	30 ºC	40 ºC	50 ºC	30 ºC	40 ºC	50 ºC
Blank	-481	-515	-530	13	15	22	0	0	0
100	-462	-483	-511	7	9	14	46.2	40.1	36.2
200	-453	-456	-484	5	7	11	61.3	53.2	50.1
300	-431	-450	-455	4	6	9	69.1	60.1	59.1
400	-420	-432	-450	3	5	8	76.5	66.4	63.4

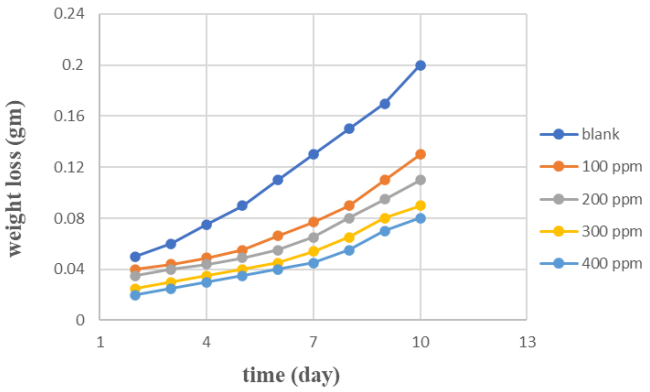

Figure 4: Weight loss and the duration of exposure to 30 °C, with or without an inhibitor.

Figure 4 shows how time and weight loss, both inhibited and non-inhibited, are related. The points follow the curve and are straight when there is no corrosion inhibitor present. Weight loss slows with increasing inhibitor doses. Figure 5 and figure 6 illustrate weight loss increases at 40 and 50 ºC whereas carbon steel corrosion rates drop at 30 ºC, which is consistent with the findings of earlier studies [15-19].

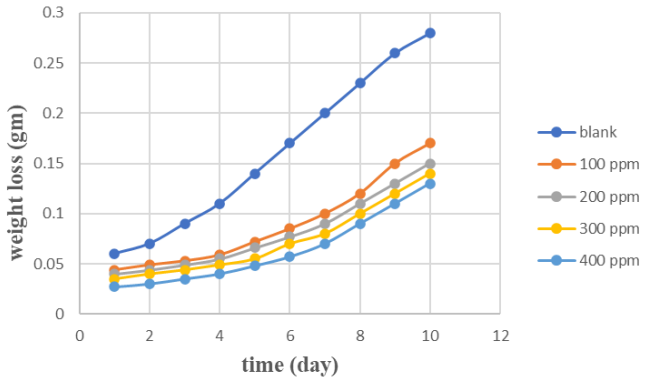

Figure 5: Weight loss and the duration of exposure to 40 °C, with or without an inhibitor.

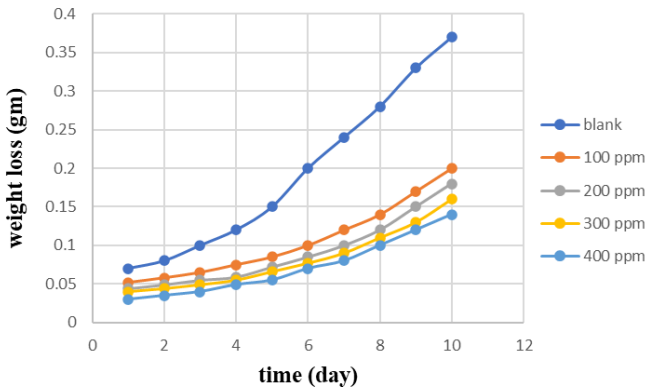

Figure 6: Weight loss and the duration of exposure to 50 °C, with or without an inhibitor

Table 2: Utilize the weight loss strategy to adjust the inhibitor concentrations at various temperatures.

Inhibitor Conc. ppm	Rate of corrosion			Efficiency of inhibition %		
	30 ºC	40 ºC	50 ºC	30 ºC	40 ºC	50 ºC
Blank	0.561	0.610	0.712	0	0	0
100	0.145	0.172	0.216	73.52	71.42	69.34
200	0.130	0.151	0.184	76.51	75.41	73.81
300	0.122	0.142	0.172	78.09	76.51	75.60
400	0.092	0.110	0.151	83.10	81.52	78.30

The efficiency of inhibitors in reducing corrosion at different temperatures and concentrations is shown in (table 2). However, figure 7 illustrates the rate of oxidation decreases and the efficiency of inhibition increases as the inhibitor concentration increases due to the inhibitors' capacity to stick to the metal's surface and encourage the formation of an additional layer of electricity. At 400 ppm and 30 ºC, low carbon steel demonstrated exceptional corrosion resistance, which is in excellent accord with the findings of other experts [12-18].

3.2 Temperature Effect

One molar hydrochloric acid solution was used to investigate how temperature affected low steel metal. Results showed that the effectiveness of corrosion prevention is impacted by the increase in temperature from 30 to 50 ºC because of elevated corrosion rates as shown in (figure 8) [14-20]. The activation energy may be computed using the following formula.

$$(C.R) = A \exp \frac{-Ea}{RT}$$

Where T stands for temperature, Ea for activation energy, R for the universal gas constant, and A for a constant.

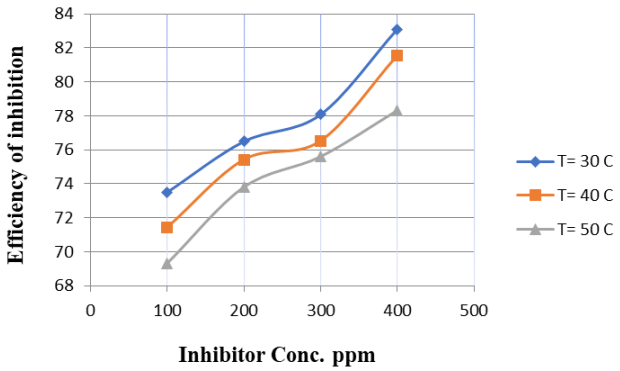

Figure 7: Plot inhibitor concentrations against effectiveness of inhibition at different temperatures.

Figures 8 and 9 can be used to compare the energy of activation of corrosion with and without inhibitors. Table 3 displays the outcomes of the thermodynamic characteristics. It has been demonstrated that the activation energy is higher when inhibitors are present than when they are absent. At increasing activation energy levels, corrosion was inhibited as the inhibitor concentration rose. The activation energy dropped with increasing temperature, but the corrosion rate remained consistent.

The thermodynamic activation energy levels, H, S, and G, were calculated using the following formula [18-21].

$$(C.R) = \left(\frac{RT}{Nh}\right) \exp \frac{\Delta S}{R} \exp \frac{-\Delta H}{RT}$$

The Plank constant, temperature, universal gas constant, and Avogadro number are denoted by letters h, T, R, and N respectively. Furthermore, enthalpy and entropy may be calculated using the following formulae for the free adsorption energy.

$$\Delta H = Ea - RT$$

$$\Delta G = \Delta H - T\Delta S$$

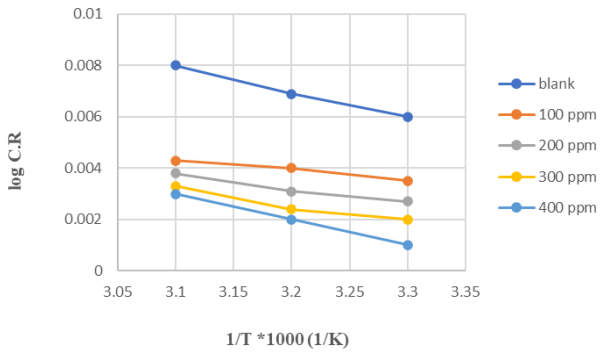

Figure 8: The inverse temperature and log C.R. at different concentrations.

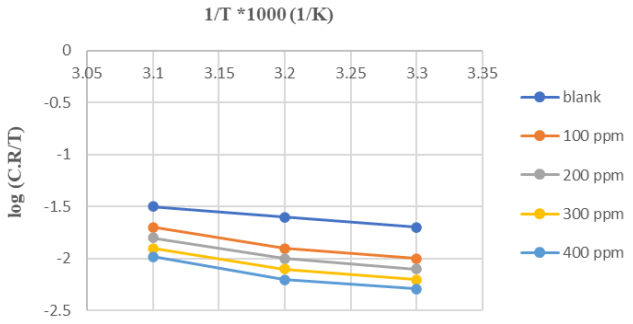

Figure 9: The inverse temperature and log (C.R./T) at different concentrations.

Table 3: Carbon steel's thermodynamic properties at 30 °C in an acidic atmosphere with varying inhibitor concentration.

Inhibitor Conc. ppm	Ea (KJ/mole)	ΔH (KJ/mole)	ΔS (KJ/mole)	ΔG (KJ/mole)
Blank	6.241	16.644	9×10^{-13}	16.644
100	2.901	6.935	2.7×10^{-13}	6.935
200	3.402	7.649	2.3×10^{-13}	7.649
300	4.071	8.428	2.1×10^{-13}	8.428
400	5.008	9.233	1.8×10^{-13}	9.233

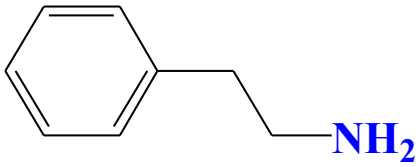

Figure10: Phenethylamine inhibitor structure.

Entropy, enthalpy, free energy of adsorption, and activation energy all increased in tandem with increasing inhibitor concentration, indicating the creation of a protective layer that may resist corrosion and shield the metal from external effects. Enthalpy levels that are positive or larger than zero indicate an endothermic system. As seen in figure 10 and findings shown in table 3, the presence of molecules containing amine and ethyl groups causes a film layer to develop on the metal surface, which in turn induces chemical adsorption and the attachment of group and atoms to the metal surface [20-25].

3.3 Computational Study

Density functional theory computations using Gaussian 09W software were used to perform quantum chemistry computations for phenethylamine as an inhibitor of corrosion under neutral circumstances. To optimize the molecular structure of phenethylamine, the 6-311G (d,p) basis set and the B3LYP technique were used.

Quantum characteristics such as the energy gap (ΔE), electron negativity (χ), hardness (η), softness (S), and number of electrons transferred (ΔN) were calculated using equations below at the same theoretical level [26-29].

$$(\Delta E = \mathrm{HOMO} - \mathrm{LUMO})$$

$$\eta = \frac{\Delta E}{2}$$

$$S = \frac{1}{\eta}$$

$$X = -\frac{1}{2}\,(\mathrm{EHOMO} + \mathrm{ELUMO})$$

$$\Delta \mathbf{N} = \frac{\chi \mathrm{Fe} - \chi \mathrm{inh}}{2(\eta\ \mathrm{Fe} + \eta\ \mathrm{inh})}$$

$$\Delta N = \frac{7 - \chi \mathrm{inh}}{2\eta \mathrm{inh}}$$

The electronegativity of iron is represented by χFe (χFe = 7 eV), the electronegativity of phenethylamine by χinx, the hardness of iron by ηFe (ηFe = 0 eV), and the hardness of phenethylamine by η inh. DFT theory was used to calculate the quantum chemical properties of phenol.

Table 4 lists molecules as strong donor, and acceptor interactions with a metal surface. The maximum occupied molecular orbital energy, HOMO = -6.66938 e V, exhibits a great ability to add electron density. Its lowest unoccupied molecular orbital energy, ELUMO = -0.494442e V, indicates the molecule's capacity to absorb electron density from the metal. The large HOMO–LUMO gap, ΔE = 6.1749 eV, reflects a compromise between chemical stability and sufficient reactivity for surface adsorption (figure 11) [26-29]. Ionization energy (IE = 6.6693 e V) and electron affinity (EA = 0.49444 eV) quantitatively confirm the dual donor-accepter nature.

The global electronegativity (χ = 3.5819) shows a little propensity to attract electrons, but the global hardness (η = 3.0874) and softness (S = 0.3239) show a moderately soft nature that promotes adsorption and charge transfer. In line with film development and adsorption-induced inhibition. The proportion of electron transfer, ΔN = 0.5534, predicts that the molecule will donate electrons to the metal surface [26-29].

Table 4: Quantum chemical parameters for phenethylamine molecules using the B3LYP technique and 6-311+G basis set.

EHOMO (a.u)	ELUMO (a.u)	ELOMO (eV)	ELUMO (eV)
-0.24509	-0.01817	-6.66938	-0.494442
ΔE	IE	EA	CP
6.1749470	6.669389	0.494442	-3.58192
ΔN	S	ω	X
0.553541	0.323889	2.07777	3.581916
Nmax	So	N	η
1.160145	0.161945	0.4812850	3.087474

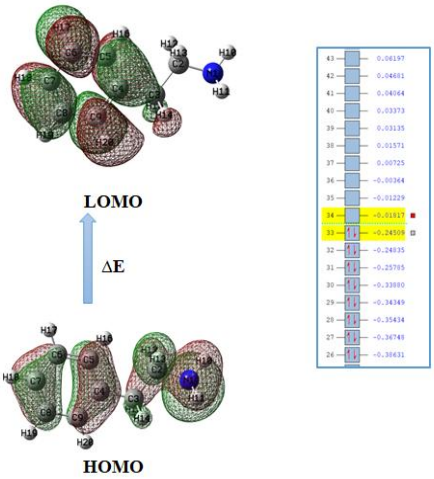

Figure 11: HOMO and LUMO of phenethylamine.

3.4 Electrostatic Potential Map

Phenethylamine molecule's electrostatic potential map is illustrated in (figure 13), shown that there are electron-poor areas scattered over several hydrogen atoms and portions of the alkyl chain. The molecular electrostatic potential map (figure 12) shows that the amine nitrogen and portions of the aromatic ring are

surrounded by electron-rich areas (negative potential).

Negative potential sites, especially the nitrogen lone pair position, are expected to be the main coordination hubs for metal binding. The HOMO/LUMO analysis's spatial distribution, which acknowledges the nitrogen in the phenyl ring and the nitrogen in the π-system as complementing donor/acceptor players that promote adsorption onto metal surfaces, further supports this [26-29].

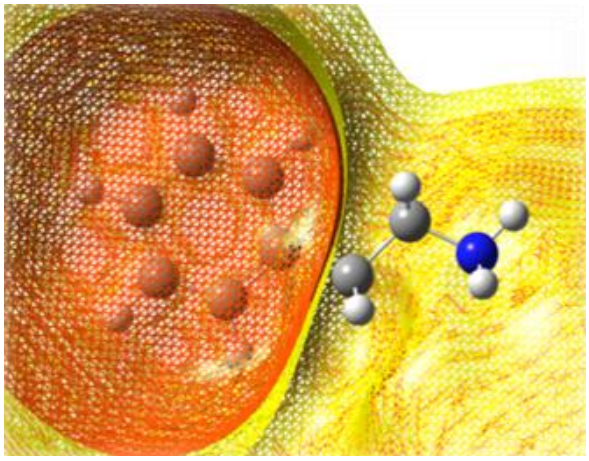

Figure12: Electrostatic potential from total SCF density.

3.5 Fukui Analysis

Distribution of reactivity sites and Fukui indices. Fukui analysis identifies the local locations of reactivity and enhances the anticipated adsorption photo. Atom 3 C (phenyl carbon) has the highest value of the nucleophilic indicator (f^- = 8.72), indicating that it is a significant electron-donating centre. The ambiphilic atom (4C) has significant f^+ and f^- values (f^+ = 0.117, f^- = 4.36), which allow it to give and receive electron density. Atoms 2, 5, and 6 likewise have significant f^- values, indicating that they are secondary electron-donating centers. Atom 1 (N, amine) possesses a moderate electronegativity (f^+ = 0.085, f^- = -0.704), which is unmatched in the electronic structure [26-29].

This enables some back donation, depending on the condition of the metal. DFT results provide the mechanism of inhibition, the nitrogen lone pair of the aromatic amine and the p-electron cloud are the primary reasons why phenolphthalein adsorbs on the metal surface. Atom 4's amphiphilia makes it easier for charges to be redistributed throughout the adsorption complex [26-29]. The powerful π resin electron donors that phenyl carbons, especially atoms 3 and 4, provide enable π–d interactions with metal d-orbitals.

The whole process involves the creation of a stabilized adsorbed coating that restricts the corrosive species' ability to reach the metal. The inhibitor then donates a net charge to the metal (positive ΔN), and the metal partially donates a charge to the inhibitor orbitals. The last step is drained at specific carbons to the non-negligible f^+.

Table 5: Mulliken population of phenethylamine.

Atoms		n	n+1	n-1	f^{+1}	f^{-1}	f^{0}
1	N	0.423778	-0.28046	0.084872	-0.70424	0.338906	-0.18267
2	C	-0.30319	-0.2848	-2.51249	0.018392	2.209301	1.113847
3	C	-0.57436	-0.64819	8.149883	-0.07383	-8.72424	-4.39904
4	C	0.996741	1.113792	-3.36217	0.117051	4.358909	2.23798
5	C	-0.75735	-0.72082	-3.66884	0.036534	2.911491	1.474013
6	C	-0.37317	-0.35009	3.792551	0.023078	-4.16572	-2.07132
7	C	-0.17359	-0.07233	-0.26263	0.101259	0.089035	0.095147
8	C	-0.14045	-0.11524	0.188165	0.025217	-0.32862	-0.1517
9	C	0.101077	0.131842	-0.12972	0.030765	0.230797	0.130781
10	H	0.224058	0.284999	0.07455	0.060941	0.149508	0.105225
11	H	0.206154	0.256558	0.001769	0.050404	0.204385	0.127395
12	H	0.142721	0.187079	0.027998	0.044358	0.114723	0.079541
13	H	0.130907	0.180771	-0.02019	0.049864	0.1511	0.100482
14	H	0.149773	0.197268	-0.0313	0.047495	0.181071	0.114283
15	H	0.180201	0.221577	-0.01749	0.041376	0.197692	0.119534
16	H	0.124189	0.168101	-0.11031	0.043912	0.234501	0.139207
17	H	0.123253	0.181659	-0.02973	0.058406	0.152987	0.105697
18	H	0.122254	0.190851	-0.00297	0.068597	0.125225	0.096911
19	H	0.124444	0.183568	-0.00036	0.059124	0.124807	0.091966
20	H	0.120114	0.173859	-0.00184	0.053745	0.12195	0.087848

4. Conclusion

Gravimetric and potentiodynamic polarization techniques were applied in this study. In one molar HCl solution, the potential of phenolphthalein to stop carbon steel corrosion at varying concentrations was examined. The inhibitor's inhibitory efficacy IE% dropped as temperature and concentration rose.

In acidic solutions, the inhibitor exhibited a high IE%. Since the inhibitor's adsorption on the metal surface creates a layer, and the structure's amine and methyl chains are necessary for the adsorption process, both polarization and loss of weight procedures produce results that are appropriate for inhibiting corrosion efficiency.

At 30 °C and 400 ppm concentration, the best results were obtained; these values are consistent with the results of several previous investigations. Phenethylamines were shown to be mixed-type inhibitors by potentiodynamic polarization tests. Adsorption and dissolution thermodynamic functions were calculated. Adsorption and dissolution thermodynamic functions have been calculated using DFT.

Quantum chemical study indicates that Phenethylamine may effectively adsorb on the iron surface by means of electron transfer and dual donor-acceptor interactions, therefore forming a persistent protective layer. The strong agreement between these theoretical findings and the practical data validates its high inhibitory efficacy. The inhibitor's theoretical state by DFT was also examined because, as previously discovered by a program, theoretical corrosion inhibition is dependent on a few variables, including electronegativity, total hardness, softness, ionization energy, dipole moment, energy gap, and the percentage of transferred electrons.

The " LUMO" energy of the lowest-occupied molecular orbital and the "HOMO" energy of the highest-occupied molecular orbital. Furthermore, the total electrostatic potential (ESP) and the inhibitor's total electron density (TED) were computed.

5. References

1. Sowmyashree A. S., Somya A., Kumar C. P., and Rao S., (2021). Novel nano corrosion inhibitor, integrated zinc titanate nano particles: Synthesis, characterization, thermodynamic and electrochemical studies. Surfaces and Interfaces. 22, 100812.
2. Al-Uqaily Raheem A. H., Khazaal F. A., and Al-Bayaty S. A., (2022). Study inhibition by 2-mercaptobenzothiazole as inhibitor and effect for carbon steel corrosion in 1M HCl solution. AIP Conference Proceedings. 2386.
3. Al-Uqaily R. A. H., Al-Bayaty S. A., Khadom A. A., and Kadhim M. M., (2022). Inhibitive performance of 4-Methoxyphenethylamine on low-carbon steel in 1 M hydrochloric acid: Kinetics, theoretical, and mathematical views. Journal of Molecular Liquids. 350, 118523.
4. Alrefaee S., Rhee K. Y., Verma C., Quraishi M., and Ebenso E., (2020). Challenges and advantages of using plant extract as inhibitors in modern corrosion inhibition systems: Recent advancements. Journal of Molecular Liquids. 321.
5. Abaies J. K., Odhafa B. R., Kathim S. H., Al-Uqaily R. A., and Al-Bayaty S. A., (2024). Effect of inhibition on low carbon steel corrosion in acidic conditions by 2-(p-tolyl) ethylamine under different conditions. In AIP Conference Proceedings. 3051, 1.
6. Thilgavathi R., Sandhiya P., Prithiba A., and Rajalakshmi R., (2019). Application of Ipomea staphylina leaf as an eco-friendly biomass for the corrosion inhibition of mild steel in 1M HCl. Materials Today Proceeding. 18, 1633-1647.
7. Pavithra M., Venkatesha T., Kanagalasara V., and Nayana K. O., (2010). Synergistic effect of halide ions on improving corrosion inhibition behaviour of benzisothiozole-3-piperizine hydrochloride on mild steel in 0.5 M H_2SO_4 medium. Corrosion Science. 52, 11, 3811-3819.
8. Singh S. K., Felse A. P., Nunez A., Foglia T. A., and Gross R. A., (2003). Regioselective enzyme-catalyzed synthesis of sophorolipid esters, amides, and multifunctional monomers. The Journal of organic chemistry. 68, 14, 5466-5477.
9. Singh K., and Quraishi M. A., (2010). Inhibiting effects of 5-substituted isatin-based Mannich bases on the corrosion of mild steel in hydrochloric acid solution. Journal of Applied Electrochemistry. 40, 7, 1293-1306.
10. Obot I., and Obi-Egbedi N., (2010). Adsorption properties and inhibition of mild steel corrosion in sulphuric acid solution by ketoconazole: Experimental and theoretical investigation. Corrosion Science. 52, 198-204.

11. Li W. H., He Q., Zhang S. T., Pei C. L., and Hou B. R., (2008). Some new triazole derivatives as inhibitors for mild steel corrosion in acidic medium. Journal of Applied Electrochemistry. 38, 3, 289-295.
12. Kuriakose N., Joby K., Raphael V., and Shanmughan S., (2014). Electrochemical Impedance Spectroscopy and Potentiodynamic Polarization Analysis on Anticorrosive Activity of Thiophene-2-Carbaldehyde Derivative in Acid Medium. Indian Journal of Materials Science. 1-6.
13. Bentiss F., Traisnel M., Gengembre L., and Lagrenée M., (2000). Inhibition of acidic corrosion of mild steel by 3,5-diphenyl-4H-1,2,4-triazole. Applied Surface Science. 161, 1-2, 194-202.
14. Yurt A., and Aykın Ö., (2011). Diphenolic Schiff bases as corrosion inhibitors for aluminium in 0.1 M HCl: Potentiodynamic polarisation and EQCM investigations. Corrosion Science. 53, 3725-3732.
15. Paul A., Joby K., Raphael V., Shanmughan S., (2012). Electrochemical and Gravimetric Corrosion Inhibition Investigations of A Heterocyclic Schiff Base Derived From 3- Formylindole. IOSR Journal of Applied Chemistry (IOSRJAC). 1. 17-23.
16. Pragathiswaran C., Ramadevi P., Kumar K. K., (2021). Imidazole and Al^{3+}nano material as corrosion inhibitor for mild steel in hydrochloric acid solutions. Materials Today: Proceedings. 37, 2, 2912-2916.
17. Fanfoon Y., Al-Uqaily R. H., Salman A., Kadhim M., Salman A., Abbas Z., Abdul Hussein E., and Fanfoon D., (2021). -Isoquinolinyl phenyl ketone as a corrosion inhibitor: A theoretical study. Materials Today: Proceedings. 42, 2241-2246.
18. Patel A. S., Panchal V. A., Mudaliar G. V., and Shah N. K., (2013). Impedance spectroscopic study of corrosion inhibition of Al-Pure by organic Schiff base in hydrochloric acid, Journal of Saudi Chemical Society. 17, 1 , 53-59.
19. Manh T. D., Hien P. V., Bau N. Q., Quyen T. N., Hinton B., and Nam N. D., (2019). Corrosion inhibition of steel in naturally aerated chloride solution by rare-earth 4-hydroxycinnamate compound. Journal of the Taiwan Institute of Chemical Engineers. 103, 177-189.
20. Haldhar R., Prasad D., Bahadur I., Dagdag O., and Berisha A., (2020). Evaluation of Gloriosa superba seeds extract as corrosion inhibition for low carbon steel in sulfuric acidic medium: A combined experimental and computational studies. Journal of Molecular Liquids. 323. 114958.
21. Odhafa B. R., Hameed S., AL-Zamili H. A. A., Al-Uqaily R. A., Al-Bayaty S. A., (2024). Verification of the physical, chemical and microbiological characteristics of the Tigris river using the water quality assessment index in Misan

Province, Iraq. In AIP Conference Proceedings. 3051, 1, 020003.

22. Anh H. T., Vu H., Huyen L. T., Tran N.Q., Thu H. T., Bach L. X., Trinh Q. T., Vattikuti S. V., and Nam N. D., (2020). Ficus racemosa leaf extract for inhibiting steel corrosion in a hydrochloric acid medium. Alexandria Engineering Journal. 59. 6.
23. Ali A. H., Abdullah A. F., Mohammed M. M., Al-Uqaily R. A., and Al-Bayaty S. A., (2024). The use of an organic compound (ethyl-2-bromothiazole-4-carboxylate) as an inhibitor to reduce the corrosion of copper in acidic media. In AIP Conference Proceedings. 3051, 1, 070008.
24. Muthukrishnan P., Jeyaprabha B., Prakash P., (2017). Adsorption and corrosion inhibiting behavior of Lannea coromandelica leaf extract on mild steel corrosion. Arabian Journal of Chemistry. 10, S2343-S2354.
25. Kathim S. H., Jasim S. B., Ali A. A., Al-Uqaily R. A., and Al-Bayaty S. A., (2024). Investigation of (4-ethylphenethylamine) as organic inhibitor for carbon steel corrosion in HCl acid under various conditions. In AIP Conference Proceedings. 3051, 1, 070003.
26. Abdullah A. F., Kathim S. H., Sager A. G., Abaies J. K., (2025). Synthesis and Identification of Two Dyes Derived from p-amino phenol and Study of their Effectiveness as Corrosion Inhibitors: Experimental and Theoretical Analysis. Baghdad Science Journal. 22, 5, 1131-1142.
27. Sager A. G., Abaies J. K., and Katoof Z. R., (2024). Synthesis of Dyes Sulfamidazole: Characterization, Evaluation, Molecular Docking and Global Descriptors by Density Functional Theory (DFT). Karbala International Journal of Modern Science. 10, 2, 11.
28. Sager A. G., Abaies J. K., Abdullah A. F., (2025). Synthesis, Antibacterial Evaluation, and Prediction of the Ability of Corrosion Inhibition by Density Functional Theory of Azo-dyes of Folic Acid, Baghdad Science Journal. 22, 6,1757-1773.
29. Sager A. G., Abbood A. F., Abaies J. K., and Khazal F. A., (2025). A Design, Molecular Docking, ADMET Studies, Synthesis, Characterization, and Invitro Pharmacological Evaluation of Tetrazole Derivatives. Iraqi Journal of Pharmaceutical Sciences. Open source preview. 34, 1, 10-25.